ADVANCED MATERIALS

Supporting Information

for *Adv. Mater.*, DOI 10.1002/adma.202212086

Direct Observation of Quadrupolar Strain Fields forming a Shear Band in Metallic Glasses

Sangjun Kang, Di Wang, Arnaud Caron, Christian Minnert, Karsten Durst, Christian Kübel and Xiaoke Mu**

Supplementary Information

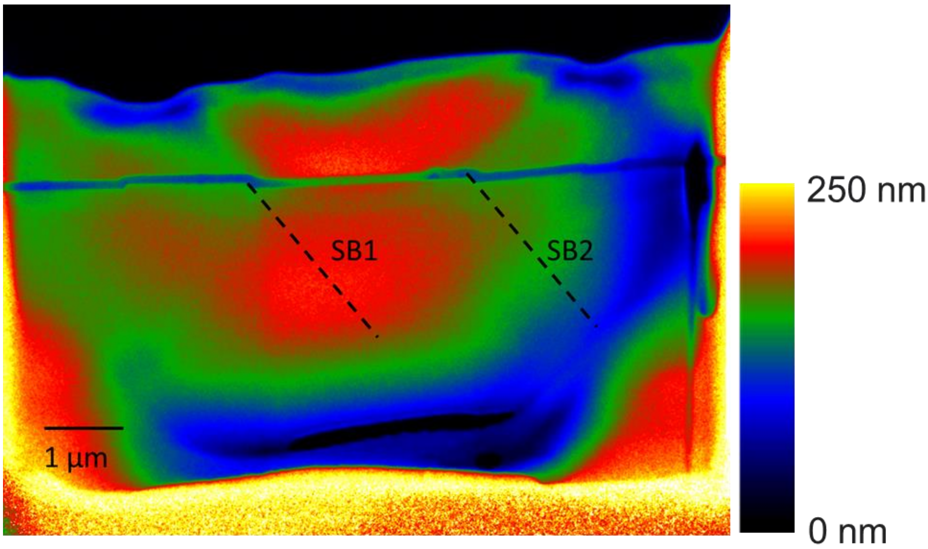

Figure S1: Thickness map of the FIB-prepared $Fe_{85.2}Si_{0.5}B_{9.5}P_4Cu_{0.8}$ metallic glass ribbon obtained from energy-filtered transmission electron microscopy (EFTEM). The mean free path (MFP) of an electron for $Fe_{85.2}Si_{0.5}B_{9.5}P_4Cu_{0.8}$ metallic glass was estimated to be ~75 nm for the thickness calculation.

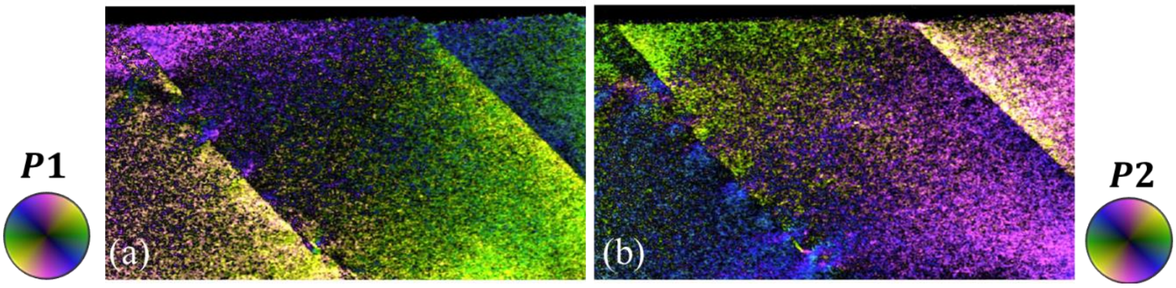

Figure S2: Deformed $Fe_{85.2}Si_{0.5}B_{9.5}P_4Cu_{0.8}$ metallic glass ribbon. (a) Principal strain P1, (b) principal strain P2.

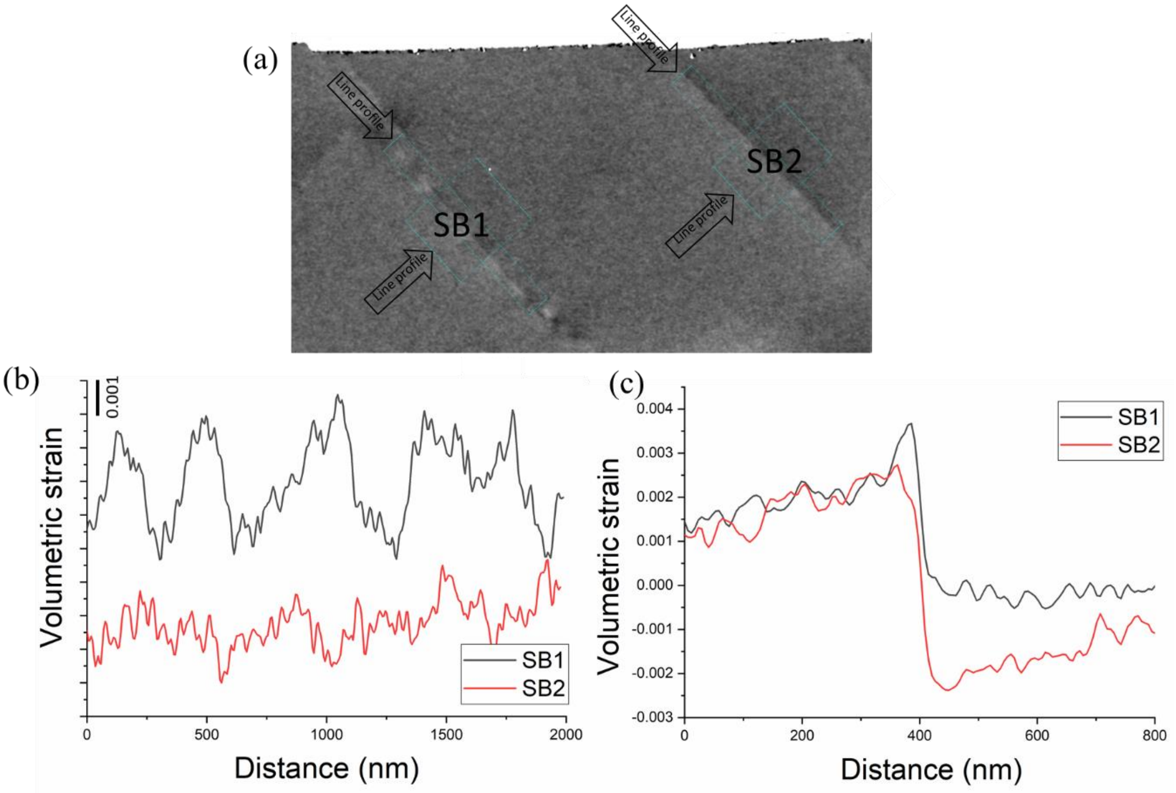

Figure S3: (a) Map of ε_{Vol} for the $Fe_{85.2}Si_{0.5}B_{9.5}P_4Cu_{0.8}$ metallic glass ribbon. (b) Line profiles taken along SB1(left) and SB2 (right) show periodic variations for SB1 and weaker variations along SB2. (c) Line profiles taken across SB1 (left) and SB2 (right) show the asymmetric strain across both shear bands.

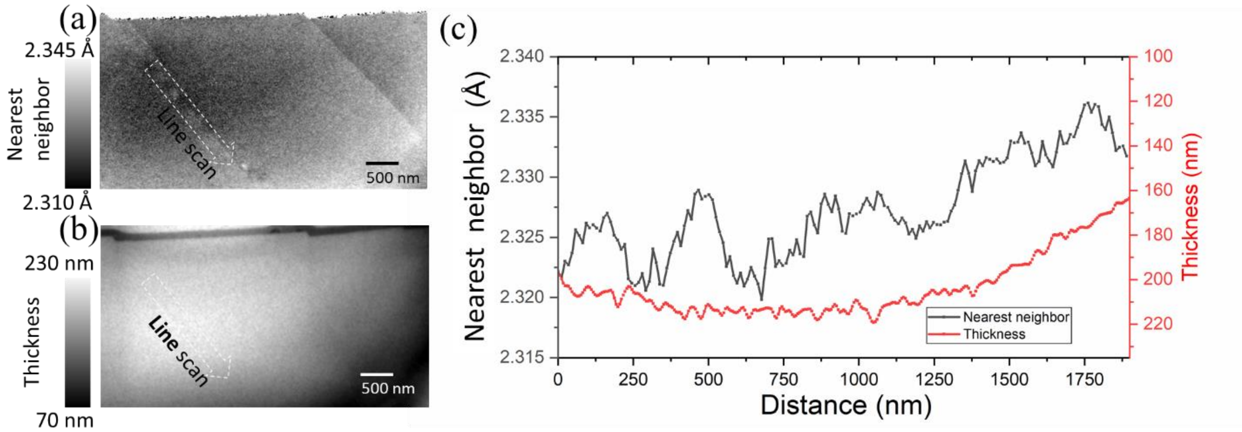

Figure S4: Influence of thickness on the PDF analysis for the deformed $Fe_{85.2}Si_{0.5}B_{9.5}P_4Cu_{0.8}$ metallic glass ribbon: (a) map of the nearest-neighbor distance, (b) thickness map, (c) line profiles of the nearest-neighbor distance and thickness along the SB indicated in (a) and (b).

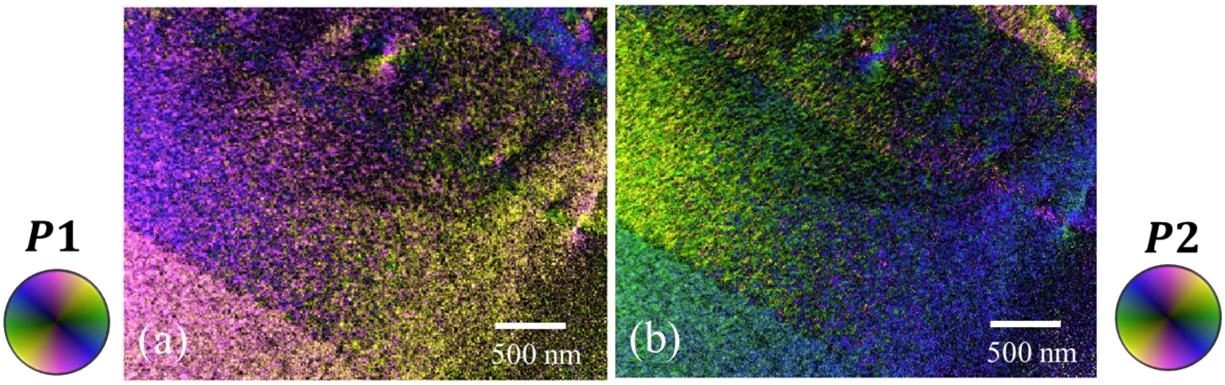

Figure S5: (a) Principal strain P1, (b) principal strain P2 of deformed $Zr_{46}Cu_{38}Al_8Ag_8$ bulk metallic glass.

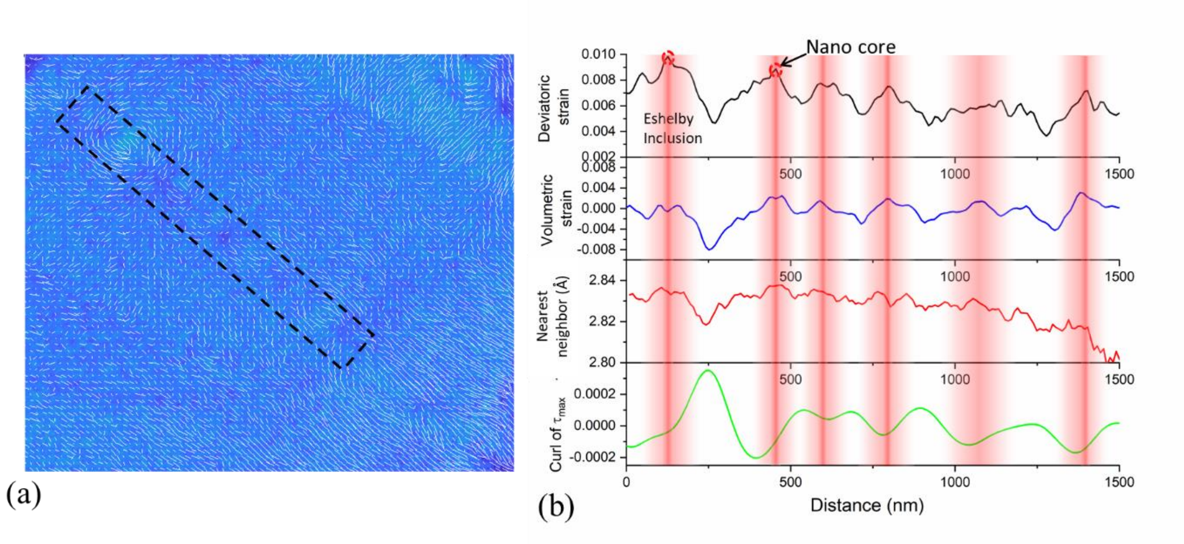

Figure S6: (a) Vector field visualization of the maximum shear strain overlayed on the map of ε_{Vol} for a $Zr_{46}Cu_{38}Al_8Ag_8$ bulk metallic glass. (b) Line profiles of the deviatoric strain, volumetric strain, nearest-neighbor distance, and curl of γ_{max} along the shear band in the region indicated by a red rectangle in (a). The red highlights indicate the position of the shear transformation inclusions.

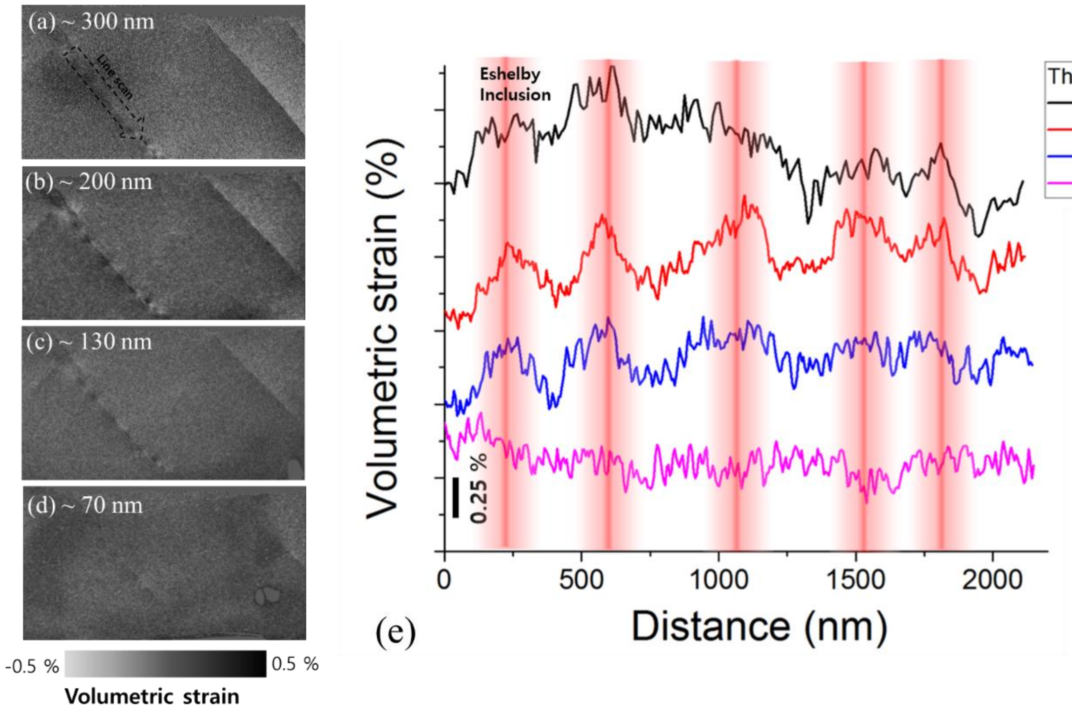

Figure S7: Strain observation for the sample at different FIB milling thicknesses prepared from the deformed $Fe_{85.2}Si_{0.5}B_{9.5}P_4Cu_{0.8}$ metallic glass ribbon. Volumetric strain map of the sample that was thinned in several steps from (a) 300 nm to (b) 200 nm, (c) 130 nm, and (d) 70 nm. The same area was mapped by 4D-STEM using identical imaging settings. (e) Line profiles of the volumetric strain maps along the SB1 for the sample with different thicknesses.

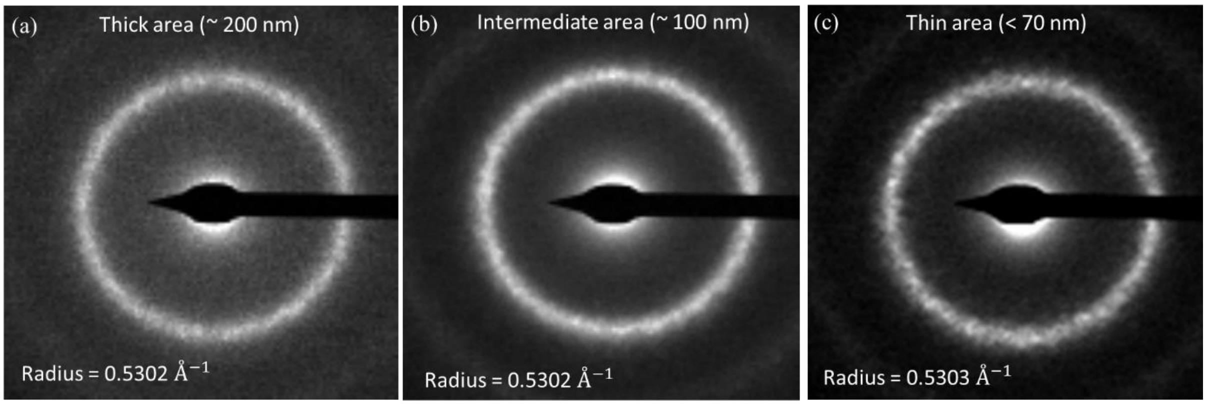

Figure S8: Single diffraction patterns of the $Fe_{85.2}Si_{0.5}B_{9.5}P_4Cu_{0.8}$ metallic glass from (a) a thick area ~ 200 nm, (b) an area with intermediate thickness, and (c) a thin area (< 70 nm) produced by stepwise thinning of the same sample.

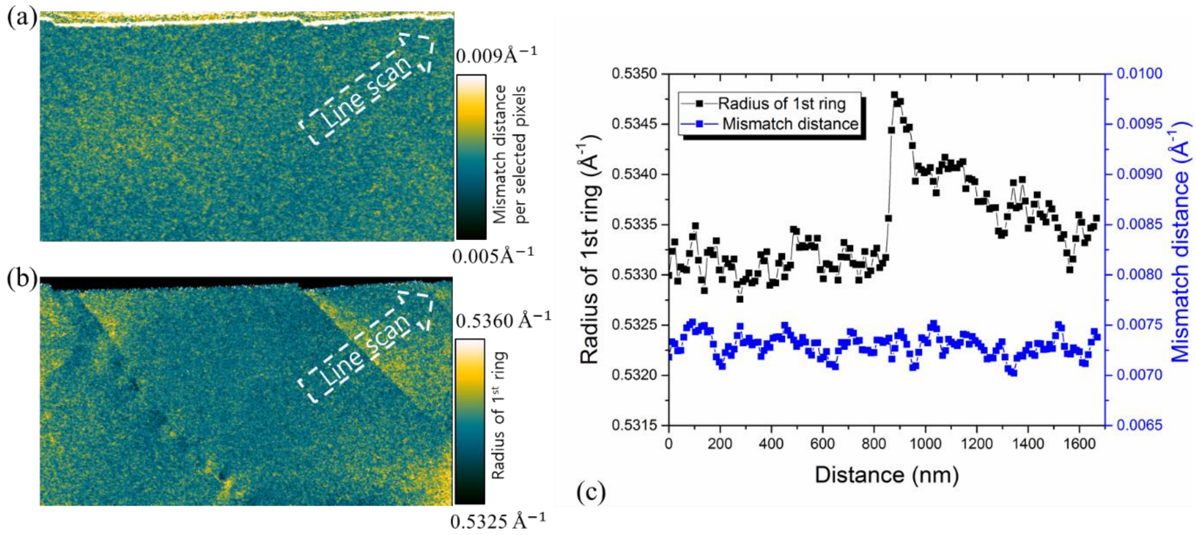

Figure S9: Statistical analysis for the accuracy of the strain measurement. (a) Map of mismatch distance per pixel for ellipse fitting for strain measurement. (b) Map of the radius of the 1st ring (q_{max}). (c) Line profiles of the mismatch distance and the radius of the 1st ring in the region indicated by white dash arrows in (a) and (b).

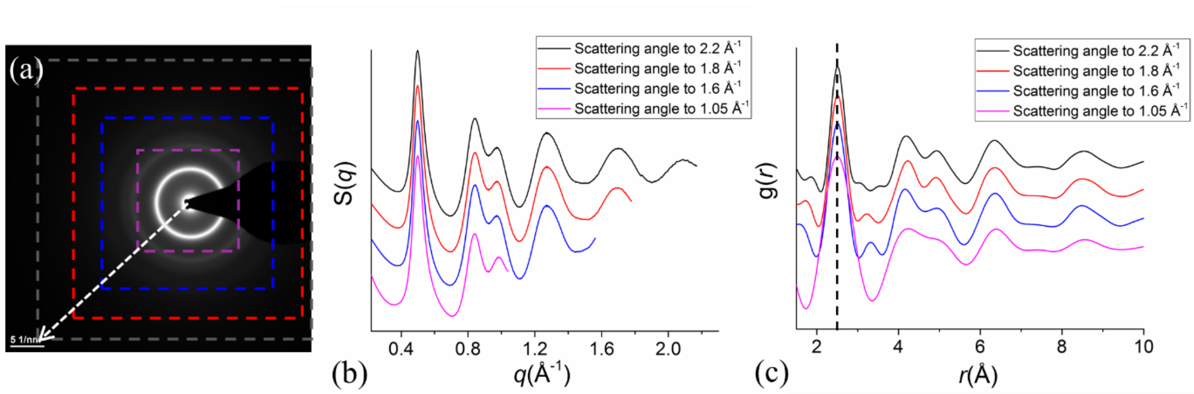

Figure S10: PDF analysis for the diffraction patterns with different maximum scattering angles. (a) Diffraction pattern of $Fe_{85.2}Si_{0.5}B_{9.5}P_4Cu_{0.8}$ metallic glass at a thickness of ~ 70 nm. The dashed rectangles indicate maximum scattering angles (virtual detector sizes). (b) S(q)s at different maximum scattering angles from 2.2 $Å^{-1}$ to 1.05 $Å^{-1}$ and (d) calculated PDFs from each S(q)s. The verticle dashed line shows the identical first peak position of PDFs.